


ORIGINAL RESEARCH

Parallel Murine and Human Aortic Wall Genomics Reveals Metabolic Reprogramming as Key Driver of Abdominal Aortic Aneurysm Progression

Gabor Gäbel, MD*¹; Bernd H. Northhoff ¹ , MSc*¹; Amanda Balboa, MSc¹; Mediha Becirovic- Agic, PhD¹; Marcelo Petri, PhD¹; Albert Busch, MD¹; Lars Maegdefessel ¹ , MD¹; Adrian Mahlmann, MD¹; Stefan Ludwig, MD¹; Daniel Teupser, MD¹; Vivian de Waard, PhD¹; Jonathan Golledge ¹ , MD¹; Anders Wanhainen, MD, PhD¹; Dick Wågsäter, PhD¹; Lesca M. Holdt, MD¹; Jan H. N. Lindeman ¹ , MD, PhD¹

BACKGROUND: While numerous interventions effectively interfered with abdominal aortic aneurysm (AAA) formation/progression in preclinical models, none of the successes translated into clinical success. Hence, a systematic exploration of parallel and divergent processes in clinical AAA disease and its 2 primary models (the porcine pancreatic elastase and angiotensin-II infusion [AngII] murine model) was performed to identify mechanisms relevant for aneurysm disease.

METHODS AND RESULTS: This study combines Movat staining and pathway analysis for histological and genomic comparisons between clinical disease and its models. The impact of a notable genomic signal for metabolic reprogramming was tested in a rescue trial (AngII model) evaluating the impact of 1-(4-pyridinyl)-3-(2-quinolinyl)-2-propen-1-one (PFK15)-mediated interference with main glycolytic switch PFKFB3. Histological evaluation characterized the AngII model as a dissection model that is accompanied by adventitial fibrosis. The porcine pancreatic elastase model showed a transient inflammatory response and aortic dilatation, followed by stabilization and fibrosis. Normalization of the genomic responses at day 14 confirmed the self-limiting nature of the porcine pancreatic elastase model. Clear parallel genomic responses with activated adaptive immune responses, and particularly strong signals for metabolic switching were observed in human AAA and the AngII model. Rescue intervention with the glycolysis inhibitor PFK15 in the AngII model showed that interference with the glycolytic switching quenches aneurysm formation.

CONCLUSIONS: Despite clear morphological contrasts, remarkable genomic parallels exist for clinical AAA disease and the AngII model. The metabolic response appears causatively involved in AAA progression and provides a novel therapeutic target. The clear transient genomic response classifies the porcine pancreatic elastase model as a disease initiation model.

Key Words: abdominal aortic aneurysm ■ angiotensin II model ■ elastase model ■ gene expression ■ glycolysis ■ human ■ metabolic reprogramming

A ruptured abdominal aortic aneurysm (AAA) is a medical catastrophe with an estimated overall mortality of 80%. Risk of rupture progressively associates with AAA diameter. As a consequence, current guidelines advise elective repair of larger (>55 mm) aneurysms.¹ Multiple trials have shown no survival benefit

for repair of smaller AAA, implying a potential for medical interventions aimed at stabilizing small AAA (“keep small aneurysms small”).^{2,3}

Remarkably, while several hundred therapies have been shown to effectively interfere with AAA formation or progression in experimental models, this

Correspondence to: Jan H. N. Lindeman, MD, PhD, Department of Surgery, Leiden University Medical Center, PO Box 9600, Albinusdreef 2, Leiden, 2300 RC, The Netherlands. E-mail: lindeman@lumc.nl

*G. Gäbel and B.H. Northhoff contributed equally as co-first authors.

Supplementary material for this article is available at <https://www.ahajournals.org/doi/suppl/10.1161/JAHA.120.020231>

For Sources of Funding and Disclosures, see page 15.

© 2021 The Authors. Published on behalf of the American Heart Association, Inc., by Wiley. This is an open access article under the terms of the Creative Commons Attribution-NonCommercial-NoDerivs License, which permits use and distribution in any medium, provided the original work is properly cited, the use is non-commercial and no modifications or adaptations are made.

JAHA is available at: www.ahajournals.org/journal/jaha

CLINICAL PERSPECTIVE

What Is New?

- In light of the lack of translatability of preclinical successes with respect to pharmaceutical abdominal aortic aneurysm stabilization, a systematic genomic and histologic exploration of parallel and divergent disease pathways in clinical abdominal aortic aneurysm disease and its 2 primaries was performed.
- Notable parallels hallmarked by metabolic responses were observed for clinical abdominal aortic aneurysm disease and aneurysms in the angiotensin-II model.
- Rescue intervention with a glycolysis inhibitor showed that interference with metabolic reprogramming quenched aneurysm formation.

What Are the Clinical Implications?

- The observations provide a rationale for the putative beneficial effects of metformin therapy as well as for the as-yet unexplained negative association between diabetic disease and abdominal aortic aneurysm progression.

Nonstandard Abbreviations and Acronyms

AngII	angiotensin-II
PFK15	1-(4-pyridinyl)-3-(2-quinolinyl)-2-propen-1-one
PPE	porcine pancreatic elastase

enormous investment has not produced any notable clinical application.⁴ In fact, there is currently no established pharmaceutical therapy for aneurysm stabilization.^{3,4} The sharp contrast between preclinical successes and clinical failures is discouraging, and may imply limited translatability of the available experimental models for clinical, late-stage AAA disease.⁴

By far the most commonly used models of AAA disease are the angiotensin-II mouse model (AngII) and the rodent “elastase” model. Aneurysm formation in the elastase model is triggered by brief porcine pancreatic elastase (PPE) exposure of an isolated infrarenal aorta segment.⁵ Exposure results in an initial, modest expansion caused by a loss of elastic recoil in response to the elastase exposure.⁶ This initial dilatation is then followed by a secondary dilatation that occurs approximately 1 week after the elastase exposure, and that is considered the actual aneurysm formation. The secondary dilatation

is thought to result from a delayed inflammatory response elicited by the elastase infusion or its consequences.⁷ The ultimately aortic dilatation in the model varies between 150 and 200%. A major criticism of the model is that the model stabilizes as result of fibrotic changes (“heals”), and generally does not associate with rupture.⁸

Aortic ruptures are an integral aspect of the so-called AngII model, the second most commonly used model of AAA disease. This model is based on the observation that chronic AngII infusion, delivered via an osmotic mini-pump, often results in aortic dilatation and rupture in hyperlipidemic mice.⁹ Although commonly referred to, and used as, an “aneurysm model,” it is now clear that the model should be characterized as a dissection model.¹⁰ Hence, it is unclear to what extent aspects of the AngII model translate to human AAA disease.

Consequently, while both models incorporate aspects of aortic dilatation, their actual mimicry with clinical AAA disease remains unclear. To address this point, and to identify potential novel targets for pharmaceutical AAA stabilization, we first performed a parallel histological and genomic evaluation to map corresponding and incongruent molecular aspects of clinical AAA disease, and its 2 most commonly used models. Results of the genomic profiling identified metabolic reprogramming as the most prominent signature of clinical AAA disease and the AngII model. Since this aspect has not been associated with AAA previously, we next devised an intervention trial, testing the impact of a rescue intervention with a glycolysis inhibitor in the AngII model.

METHODS

The data that support the findings of this study are available from the corresponding author upon reasonable request. Gene expression data have been deposited at Gene Expression Omnibus under the GEO accession number GSE153097.

Histological and Immunohistochemical Analysis

Histological samples in this study were from the Leiden University Medical Center tissue repository (human AAA and control samples) and previously reported studies applying the PPE model⁶ and the AngII model.¹¹ Movat pentachrome staining was performed according to the protocol in supplement 1. Stained slides were scanned at 400x magnification using Philips’ IntelliSite Ultra-Fast Scanner (Philips, Eindhoven, The Netherlands) and representative sections are shown.

Genomic Responses

Patients

AAA specimens were obtained from a total of 31 patients undergoing elective open AAA repair. Maximum infrarenal aortic diameter (mm) was assessed in patients with AAA from axial computed tomography angiography images. Control aortic tissue samples were harvested from 9 brain-dead organ donors. Patient characteristics are shown in Table 1.

Full-thickness AAA biopsies were obtained from the anterior aneurysm sac or from the infrarenal aorta of organ donors and snap-frozen in liquid nitrogen. Specimens were collected and stored at -80°C until assayed. Use of human vascular tissues was approved by the ethics committee of the Medical Faculty Dresden University (EK 316122008). The protocol conformed to ethical guidelines of the Declaration of Helsinki.

Sample collection and handling of the deceased donor aortic wall samples (controls) was in accordance with the guidelines of the Medical and Ethical Committee of the Leiden University Medical Center, and the code of conduct of the Dutch Federation of Biomedical Scientific Societies. In all cases permission for transplantation-oriented research was given or permission was inherent to donation.

AngII Mouse Model

Evaluation of the genomic responses of this model was based on deposited data from experiments performed by Rush et al.¹² Male ApoE^{-/-} mice aged 13 weeks were exposed to AngII (1.44 $\mu\text{g}/\text{kg}$ per minute; $n=5$) or saline ($n=6$) via an osmotic mini-pump (Model 2004, ALZET, Durect Corporation, Cupertino, CA, USA) for 4 weeks. After 28 days of infusion, mice were euthanized by carbon dioxide asphyxiation, the aortas were

perfused with RNAlater (Qiagen, Doncaster, Victoria, AUS), and aortic aneurysms formed were harvested, and stored at -80°C until further analysis.

AngII-induced aortic aneurysm samples for histological evaluation were positive controls from a previously reported intervention study.¹² The study was performed in 16-week-old ApoE^{-/-} mice fed a Western-type diet (containing 15% cacao butter, 1% corn oil, and 0.25% cholesterol) (Arie Blok, Woerden, The Netherlands). The diet was initiated 4 weeks before mini-pump placement and continued until the end of the experiment. AngII-containing osmotic mini-pumps were placed under inhalation isoflurane anesthesia (Baxter, IL, USA). The mini-pumps (Alzet, DURECT Corporation, Cupertino, CA, USA) released AngII (Sigma-Aldrich, St. Louis, MO, USA) with a pump-rate of 1.44 mg/kg per day. Aortas were harvested after 31 days of AngII infusion under full anesthesia, and perfused under slight pressure via the heart with 10 mL ice cold PBS for 1 minute. Thereafter, aortas were perfusion fixed via the heart with 5 mL 4% paraformaldehyde (1 minute). Incisions in the liver facilitate perfusion.

PPE Mouse Model

Experiments were approved by the administrative panel on laboratory animal care of the Karolinska Institute (N119/15) and performed as previously described.^{13,14} Ten-week-old male C57BL/6J mice were divided into 3 groups: (1) Control group ($n=4$), where animals received saline infusion in the infrarenal aortic segment, and the aorta was harvested after 7 days; (2) Elastase 1 week ($n=4$), where animals received PPE infusion in the infrarenal aortic segment, and the aorta was harvested after 7 days; and (3) Elastase 2 week ($n=4$), where animals received PPE infusion in the infrarenal aortic segment, and the aorta was harvested after 14 days. All mice were euthanized by carbon dioxide asphyxiation, the aortas perfused with RNAlater (Qiagen, Hilden, Germany), and harvested from renal arteries to iliac bifurcation and stored at -80°C until further analysis. Formalin-fixed paraffin-embedded samples for the histological evaluation of day 28 represent control samples from a separate study.

Total RNA was extracted from murine aortic samples of the PPE mouse model using the TRIzol reagent (Sigma) and was purified using RNeasy Micro Kit (Qiagen, Hilden, Germany) according to manufacturer's instructions before transcriptome analyses.

Transcriptomic Profiling

Transcriptome-wide expression analysis of the human samples was performed using the Illumina (San Diego, CA) HumanHT-12 v4 Expression BeadChip platform comparing control aortic tissue samples ($n=9$, GEO

Table 1. Patient Characteristics for Human Array Samples

Characteristic	Study Cohort (Array)		
	AAA	Controls	P Value
N	31	9	
Age, y	69.5 \pm 7.2	68.4 \pm 4.5	ns
Male sex	97%	67%	0.0299
Body mass index	27.2 \pm 3.3	...	
Max. aortic diameter (mm)	62.3 \pm 12.1	...	
Coronary artery disease	58.1%	...	
Arterial hypertension	93.5%	...	
Diabetes mellitus	32.3%	...	
Dyslipidemia	77.4%	...	
(Ever) smoking	58.1%	...	

AAA indicates elective abdominal aortic aneurysm; and ns, not significant. Nominal variables are presented in percent; continuous variables are presented as mean \pm SD. Continuous variables were compared using Mann-Whitney *U* test; nominal variables were compared using Fisher exact test.

accession GSE57691)¹⁵ and aortic tissue samples with electively treated aneurysms (n=31, GEO accession GSE98278).¹⁶

Expression profiling of the murine AngII model was performed based on publicly available raw data of Rush et al.¹² (GEO accession GSE12591) comparing the gene expression (Illumina MouseWG6 v1.1 bead chips) of murine aortas exposed to saline infusion for 4 weeks (n=6) and aortic aneurysms formed after 4 weeks angiotensin exposure (n=6; suprarenal diameter 2.06 ± 0.48 mm).

All microarray data were analyzed using the limma package in R software version 3.2.17.¹⁷ Data were background corrected and quantile normalized. Differential expressions were calculated using gene-wise linear models. Moderated t-statistics were used for significance analysis, and Benjamini and Hochberg's method to control the false discovery rate was used to correct for multiple testing as implemented in the limma package.

To map the genomic responses of the PPE model, we compared aortic RNA-Seq data from sham-operated mice (n=4) and aortas harvested, respectively, 1 week after (n=4) or 2 weeks (n=4) after PPE exposure. To this end, 500 ng of total RNA was used for library synthesis with the TrueSeq RNA Sample Prep Kit v2 (Illumina, San Diego, CA, USA). Cluster generation was performed with a concentration of 10 nM using an Illumina cBot. Sequencing of 2×100 bp was performed with an IlluminaHighScan-SQ sequencer at the sequencing core facility of the IZKF Leipzig (Faculty of Medicine, University Leipzig) using version 3 chemistry. Raw reads were mapped to the reference genome mm10 using split-read mapping algorithm implemented in segemehl.¹⁸ Mapped reads were annotated according to RefSeq database and counted using featureCounts.¹⁹ Differential expression was computed using DESeq2 algorithm.²⁰

Principal Component Analyses

Principal component analysis was performed to prove separation of the study groups based on the first 2 principal components explaining most variance of transcriptomic data, because of small sample sizes. Transcriptomic data were not adjusted for these principal components.

Pathway and Comparison Analyses

Genomic responses were mapped using Ingenuity Pathway Analysis²¹ (QIAGEN Inc., <https://www.qiagenbioinformatics.com/products/ingenuity-pathway-analysis>) considering differentially expressed genes with an absolute log₂ fold-change ≥ 1 and adjusted *P* value < 0.05 .

Gene Set Enrichment Analysis

Gene set enrichment analysis was performed using the fgsea package²² based on hallmark gene sets of the Molecular Signatures Database v7.2.^{23,24} Genes were ranked by *P* value of differential expression analysis multiplied by the sign of the fold change. Minimum and maximum gene set size was set to 15 and 500 by default. Enriched pathway were filtered by adjusted *P* values < 0.05 according to the Benjamini-Hochberg procedure.

PFK15 Intervention Study

Experiments were approved by the Animal Experiments Ethical Committee, Uppsala, Sweden. Nine- to 10-week-old male ApoE^{-/-} mice (Charles River, Italy) were divided in 3 groups. One reference group (n=6) received saline infusion, and the other 2 groups received an infusion of 1000 ng/kg per minute AngII (mini osmotic pump, Model 1004; Alzet, Cupertino, CA, USA).

AngII-infused animals were either treated with the 6-phosphofructo-2-kinase/fructose-2,6-biphosphatase 3 (PFKFB3) inhibitor 1-(4-pyridinyl)-3-(2-quinolinyl)-2-propen-1-one (PFK15)²⁵ (25 mg/kg, Cat.no.S7289, Selleckchem, Houston, TX, USA) (intervention group, n=12), or with vehicle (control group, n=14), intraperitoneally 3 times a week for 3 weeks. Treatment was started 1 week after start of the AngII infusion. Body weight was recorded throughout the study, and blood glucose monitored 3 days after the last dose of PFK15 or vehicle. Animals were housed in a controlled environment with free access to normal pelleted food and water.

Maximal aortic diameter was assessed 4 weeks after pump implantation through abdominal ultrasound (Vevo 1100 ultrasound, VisualSonics, Amsterdam, The Netherlands) in B-mode. AAA was defined as an aortic diameter > 1.5 mm. Next, mice were euthanized, the aorta was dissected for visual confirmation of aneurysm formation, and then divided in 2 segments: 1 segment frozen in OCT for histological evaluation, and the other stored in RNA-later (Qiagen Vedbæk, Denmark) at -80°C .

Total RNA was extracted from aortic tissue using RNeasy Mini Kit (Cat. no. 74104; Qiagen) and treated with RNase-free DNase (Cat. no 79254, Qiagen). RNA quality was assessed by the A260/280 ratio (NanoDrop 2000/2000c, ThermoFisher Scientific, Stockholm, Sweden and cDNA prepared using SuperScript III First-Strand Synthesis SuperMix for quantitative reverse transcription polymerase chain reaction [Cat. no.11752-050, Invitrogen, ThermoFisher Scientific]). Gene amplification was performed using QuantStudio5 (Applied Biosystems), TaqMan Gene Expression Assays probes and primers (Table 2,

ThermoFisher Scientific). Tata-box binding protein was used for normalization. Relative quantification of gene expression was performed using the $2^{-\Delta\Delta Ct}$ method.²⁶

Statistical analysis of the intervention study was performed with the GraphPad Prism 8.4 software. Results are presented as medians with interquartile range. Chi-square test was applied to evaluate possible differences in the incidence of aneurysm formation. Aorta diameters were log transformed, and compared using 1-way ANOVA followed by Fisher LSD post hoc test. Gene expression data were analyzed by unpaired *t* tests. Values of *P*<0.05 were considered statistically significant.

RESULTS

Histopathological Evaluation

Histopathological characteristics of human AAA and the PPE and AngII models are shown in Figures 1A through 1C. As a reference, Movat staining for a normal human infrarenal aorta is provided in Figure 1D. Human AAA wall is characterized by a mural thrombus (Figure 1A) and a fully remodeled aortic wall with extensive fibrotic changes, full loss of elastic laminae and

medial smooth cells (Figure 1A through 1b), presence of follicle-like structures (Figure 1A through 1c), neovascularization, and adventitial fatty degeneration (Figure 1A through 1d). The earliest phases of the PPE-induced AAA (day 1) are characterized by focal destruction of elastic lamellae (Figure 1B). An intraluminal thrombus may present in the early phase, possibly as a result of PPE-induced hypercoagulability²⁷ (Figure 1B). Day 7 lesions are characterized by a massive medial/adventitial leukocyte infiltration, which regresses in time (day 14) and is fully resolved at day 28 (Figure 1B). The aortic tissue shows signs of scarring (fibrosis), and there are no signs of a healing response with re-establishment of the normal vascular architecture.

Movat staining for an “aneurysm” formed in the AngII model (Figure 1C) revealed localized rupture of the elastic lamellae, and presence of a large intramural hematoma (dissection) with overt signs of reorganization (neovascularization, matrix disposition). The adventitial layer is hallmarked by extensive remodeling with deposition of a collagenous matrix and abundant microvessels.

Genomic Signatures of Clinical AAA Disease and the Elastase and AngII Models

Gene expression analysis followed by Ingenuity pathway profiling was applied to identify parallel and incongruent genomic signatures of clinical AAA and the 2 models. Principal component analyses on the data sets showed full separation of the 4 study groups, indicating that the group sizes provide adequate separation (Figures 2A through 2D).

We have identified 1069 genes to be differentially up-regulated in human AAA samples, 696 in samples of the PPE model at day 7, 107 at day 14, and 611 in samples of the AngII model at day 28. In parallel, 1918 differentially downregulated genes were identified in human AAA, 443 in the PPE model at day 7, 46 at day 14, and 643 for the AngII model at day 28. We found 7.3% of genes differentially expressed in human AAA samples to be also regulated in the PPE (day 7) model and 6.0% to be also regulated in the AngII model (Figures 3A through 3D).

Profiling of the genomic response of clinical AAA disease illustrated the complexity of the AAA disease (Figures 4A through 4D and 5). The disease is characterized by a broad activation of inflammatory pathways (including aspects of both the innate and adaptive immune system, as well as general proinflammatory pathways), and by enrichment of pathways and gene classes associated with cell organization, trafficking, and cell cycle/cell death (Figures 4–6). The quantitatively most notable differences between AAA and control aorta were observed for metabolic clusters,

Table 2. Probes/Primers Used to Evaluate the Impact of PFK15 Intervention on Aortic Wall Gene Expression

Gene	Probes and Primers, TaqMan Gene Expression Assays (20X), Assay ID
α-Smooth muscle cell actin (ASMA)	Mm01546133_m1
Cluster of differentiation (CD) 3e	Mm00599683_m1
Cluster of differentiation (CD) 68	Mm03047343_m1
Collagen 1A1 (ColA1)	Mm00801666_m1
Collagen 3A1 (Col3A1)	Mm01254476_m1
Cytochrome C oxidase subunit 7A1 (Cox7A1)	Mm00438296_m1
Cathepsin S (CTSS)	Mm00457902_m1
Cathepsin K (CTSK)	Mm00484036_m1
Elastase, neutrophil expressed (ELANE)	Mm00469310_m1
Fructose-1,6-bisphosphatase 1 (FBP1)	Mm00490181_m1
Interleukin-6 (IL6)	Mm00446190_m1
Matrix metalloproteinase 2 (MMP2)	Mm00439508_m1
Matrix metalloproteinase 9 (MMP9)	Mm00600163_m1
Matrix metalloproteinase 12 (MMP12)	Mm00500554_m1
Matrix metalloproteinase 14 (MMP14)	Mm00485054_m1
NADH dehydrogenase 1β subcomplex subunit 9 (NDUFB9)	Mm00612543_m1
Phosphatase and tensin homolog (PTEN)	Mm00477208_m1
Transgelin (TAGLN)	Mm00441660_m1
TATA-box binding protein (TBP)	Mm00446973_m1
Vimentin (VIM)	Mm01333430_m1

PFK15 indicates 1-(4-pyridinyl)-3-(2-quinolinyl)-2-propen-1-one.

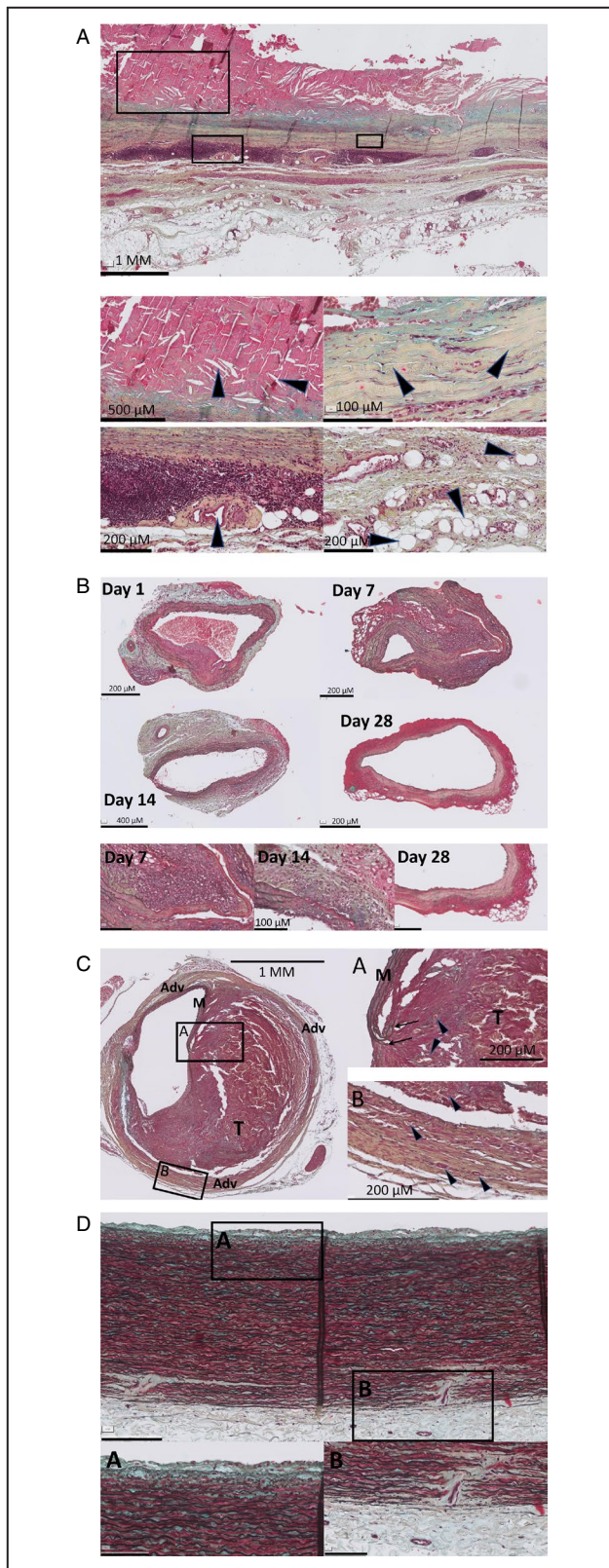


Figure 1. Histomorphology (Movat pentachrome staining) of (A) human AAA and control aorta; (B) porcine pancreatic elastase (PPE)-mediated aortic injury; (C) aortic dilatation in the angiotensin II model; and (D) normal human infrarenal aorta (reference).

A, Human AAA and control aorta. Human AAA is often accompanied by a mural thrombus (panel 1Ai of note: fibrin stains red in the Movat staining) with cholesterol clefts (indicated by arrowheads) presumably reflecting accumulation of free cholesterol from erythrocyte membranes. A discriminative aspect of AAA and aortic atherosclerotic disease is the loss of the normal 3-layered architecture, full remodeling of the media with loss of elastic lamellae and smooth muscle cells, and deposition of a collagenous, proteoglycan poor matrix (arrowheads) in AAA disease (panel 1Aii). The disease is further characterized by large tertiary infiltrates at the level of the vasa vasorum network (arrowhead) in the former outer media (panel 1Aiii), and by extensive angiogenesis and fatty degeneration (arrowhead, panel 1Aiv). **B**, Porcine pancreatic elastase (PPE)-mediated aortic injury. Day 1: Histological changes following brief (≈ 10 minutes) PPE exposure at day 1: disruption of elastic lamellae and localized intimal thickening (arrow), diffuse leucocyte infiltration in the adventitia. The adhering luminal thrombus could reflect of activation of the coagulation cascade by PPE day 7. Massive localized leukocyte infiltration in the medial and adventitial layer in the areas of elastic fiber damage (see detail day 7). Day 14: Resolution of inflammation but absent elastic lamellae (see detail day 14, arrow). Day 28: Quiescent scar with loss of the normal medial architecture (elastin/smooth muscle cell units) and fibrous changes in the inner media (see detail day 28). **C**, Aortic dilatation in the angiotensin II model. The image clearly illustrates the dissection-type dilatation in a late stage (day 28) of the AngII model. The left aspect of the aorta appears normal with a thin intima and a media with intact elastic lamellae. The adventitia (Adv), on the other hand, shows signs of fibrosis. The right aspect of the vessel shows a dissection of the media (M) with disruption and retraction of the elastic fibers (arrows in panel 1Ci), a large intramural thrombus (T) with neo-angiogenesis (microvessels indicated by the arrowheads in panel 1Ci), and an intact adventitial layer with clear signs of fibrosis (collagen deposition) (coarse yellow-ochric fibers in the Movat staining) indicated by the arrowheads in panel 1Cii). **D**, Normal human infrarenal aorta (reference). **Di**, Thin, proteoglycan-rich intima (blue-ish). **Dii**, Medial adventitial border zone with a vasa vasorum infiltrating the media. Legend for the Movat staining: black: elastin, yellow: collagen, blue: proteoglycans, green: colocalization of collagen and proteoglycans, red: smooth muscle cells/fibrin, purple: leukocytes. AAA indicates abdominal aortic aneurysm.

illustrating an apparent metabolic reprogramming with downregulation of genes associated with oxidative phosphorylation in AAA disease (Figures 4A through D and 5).

Parallel comparisons of the genomic signals of human AAA and its 2 models are provided in Figure 4. Evaluation of the genomic responses in the PPE model revealed a clear expression signature for day 7, but full normalization of the genomic signals at day 14 following elastase exposure (Figure 2D). Responses for day 7 were largely dominated by activation of pathways associated with adaptive immune- and general inflammatory (interleukin 6 and interleukin 8 [CXCL-8, mouse equivalent: KC]) responses. Although the identified pathways in the PPE model showed partial overlap with those found differentially regulated in human AAA,

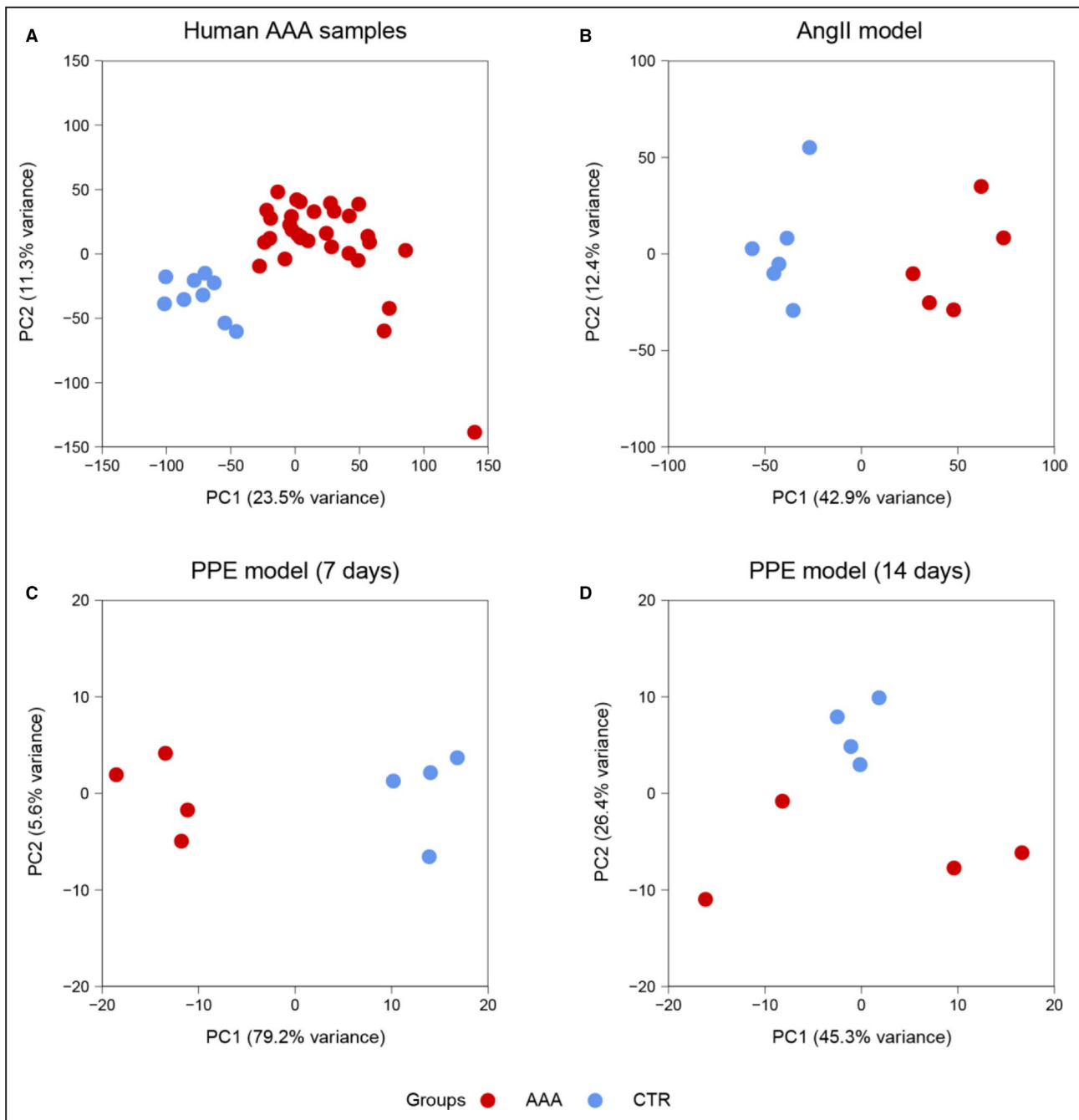


Figure 2. Principal component analysis of transcriptomic data.

All analyses revealed clear separation: the AAA samples to their controls (A), for the AngII model (day 28) to their controls (B), and for the PPE model at day 7 (C), but not for the PPE model at day 14 (D). AAA indicates abdominal aortic aneurysm; AngII, angiotensin II; CTR, controls; and PPE, porcine pancreatic elastase.

their predicted directions often contrasted with those for clinical AAA and the AngII model (Figures 4 and 5).

In contrast to the conclusions for the PPE model, partial alignment was observed for pathways differently regulated in aneurysms formed in the AngII model and clinical AAA disease, in particular, parallel dominance of pathways associated with metabolic reprogramming,

as well as enrichment of pathways associated with the adaptive immune response. (Figures 4A through D and 5) Contrasting directions were observed for pathways associated with the innate immune response and cell trafficking (ie, pathways categorized as “Leukocyte Extravasation Signaling” and “Dendritic Cell Maturation”) were predicted to be enriched in the

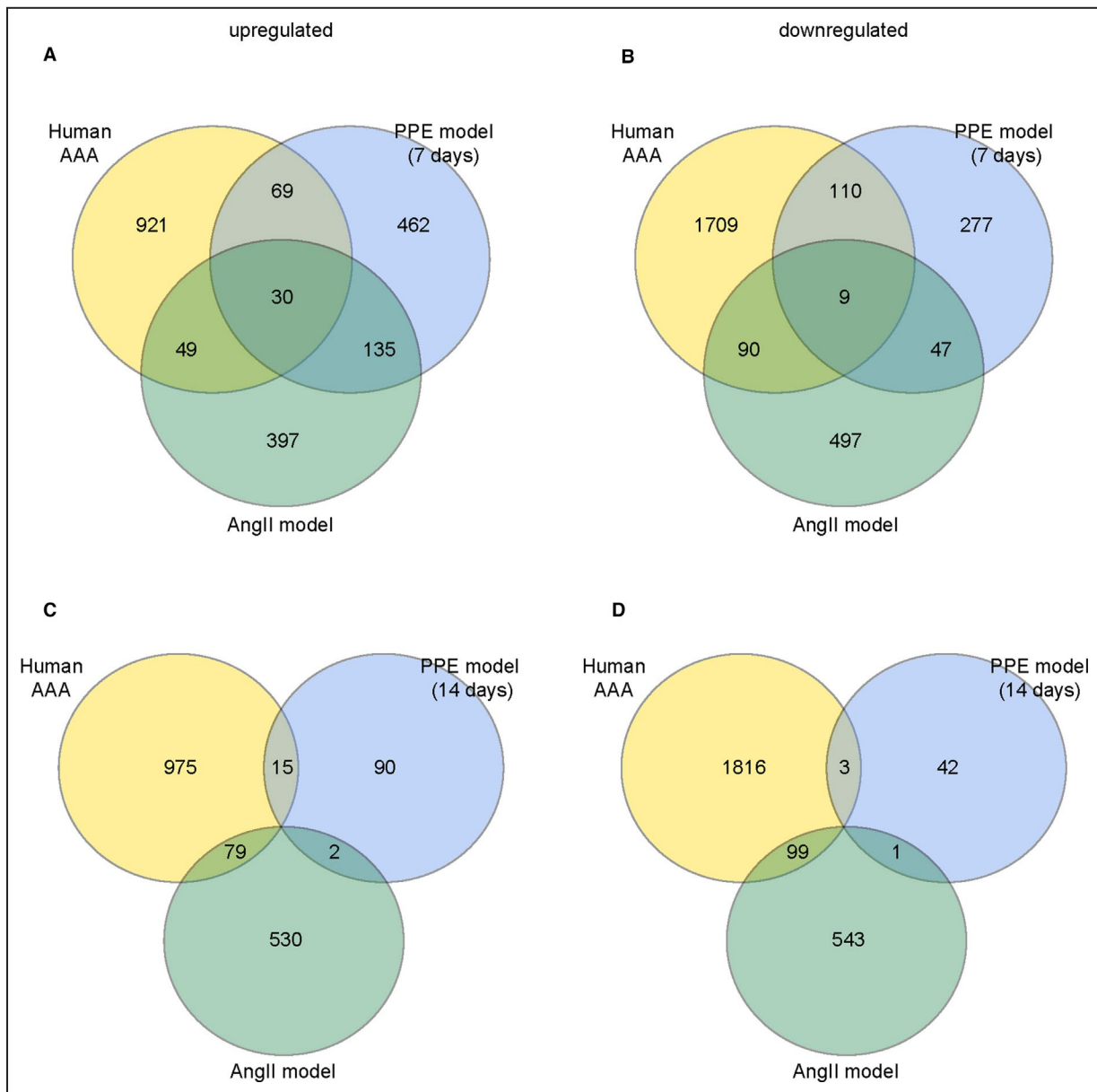


Figure 3. Venn plots of overlapping differentially expressed genes.

A, Overlap of upregulated genes for human AAA, PPE model at day 7, and AngII model. **B**, Overlap of downregulated genes for human AAA, PPE at day 7, and AngII model. **C**, Poor overlap of differentially expressed upregulated genes for the PPE model (14 days after infusion) compared with human AAA and the AngII model because of almost normalization of gene expression. **D**, The same applies to downregulated genes for the PPE model at day 14. AAA indicates abdominal aortic aneurysm; AngII, angiotensin II; and PPE, porcine pancreatic elastase.

AngII model, but were relatively suppressed in clinical AAA disease (Figure 4).

On the basis of the genomic responses, the global image appears to be that the PPE model is characterized by an acute, transient immunologic/inflammatory (“initiation”) response, while the AngII model (in alignment with clinical AAA disease) merely reflects a chronic inflammatory (“remodeling”) response with a shared dominance of gene clusters associated with metabolic reprogramming. In the light of this remarkable dominance, we performed a focused

comparison of the activation status of the metabolic master switches (Figure 7). This evaluation revealed a sharp contrast between clinical AAA disease and the AngII model on the 1 hand, and the PPE model on the other.

Notwithstanding, contrasts were also observed between human AAA and the AngII model such as contrasting predicted directions for phosphoinositide 3-kinase/protein kinase B signaling and an absent signal for AMP-activated protein kinase signaling in clinical AAA. The predicted changes in the hypoxia-induced

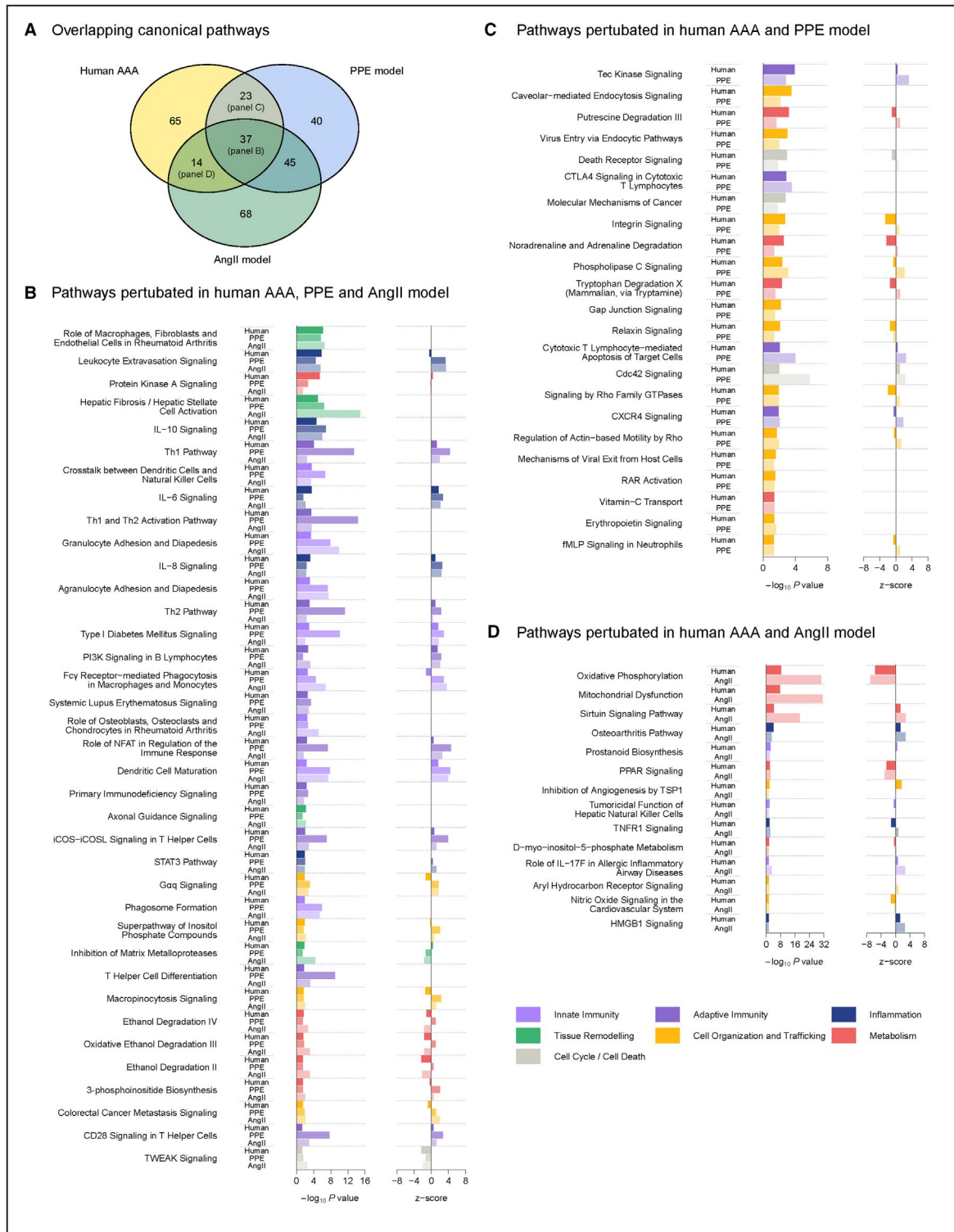


Figure 4. Comparison of the genomic responses in human AAA and the 2 AAA models

A, Venn plot illustrating the distribution of the differently activated pathways in the 3 groups. **B–D**, The significances and, if available, z-scores (Ingenuity pathway analysis) for pathways pertubated in, respectively, human AAA and the PPE and AngII models (**B**); human AAA and day 7 of the PPE model (**C**), and human AAA and the AngII model (**D**). AAA indicates abdominal aortic aneurysm; AngII, angiotensin II; CTLA4, cytotoxic T-lymphocyte –associated antigen 4; CXCR4, C-X-C Motif Chemokine Receptor 4; fMLP, n-formyl Methionyl-Leucine-Phenylalanine; HMGB1, high-mobility group box 1; ICOSL, Inducible T-cell Costimulator Ligand; IL-6, interleukin 6; IL-17, interleukin 17; IL-10, interleukin 10; NFAT, Nuclear Factor of activated T-cells; PI3K, phosphoinositide 3-kinase; PPAR, peroxisome proliferator-activated receptors; PPE, porcine pancreatic elastase; RAR, Retinoic Acid Receptor; STAT3, Signal Transducer and Activator of Transcription 3 ; Tec, Tec protein tyrosine kinase; TNFR1, Tumor Necrosis Factor Receptor 1; TSP1, Thrombospondin 1; and TWEAK, TNF superfamily member 12.

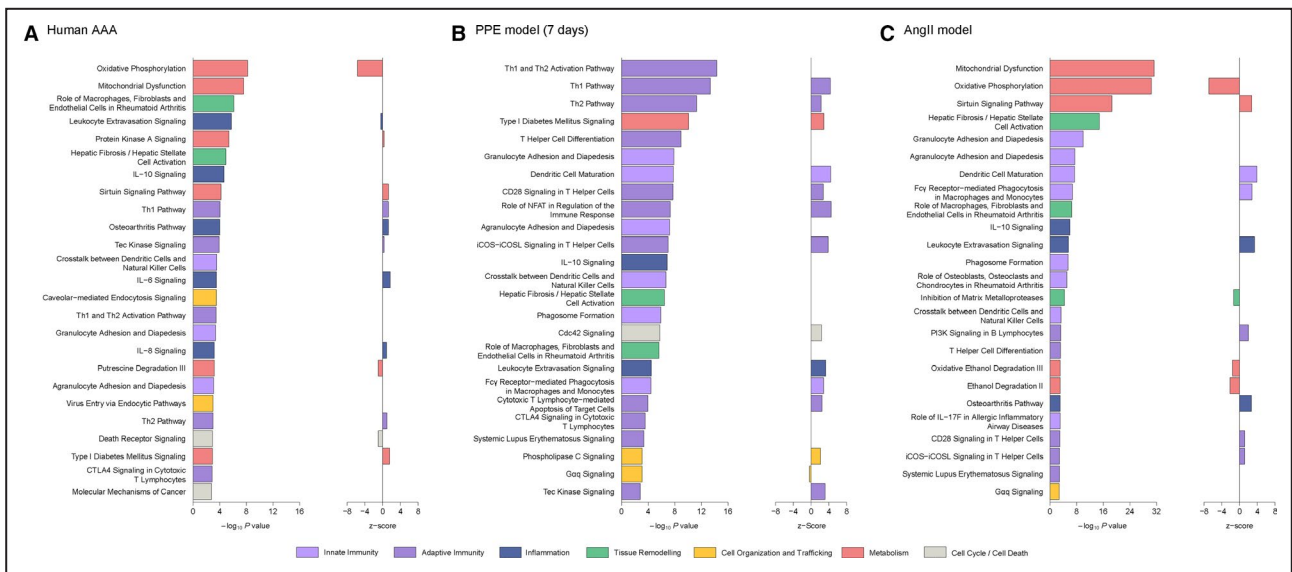


Figure 5. Top 25 differentially regulated pathways.

Significance and activation of top differentially regulated pathways in human AAA (A), day 7 in the PPE model (B), and day 28 in the AngII model (C). AAA indicates abdominal aortic aneurysm; AngII, angiotensin II; CD26, Cluster of Differentiation 26; CTLA4, cytotoxic T-lymphocyte-associated antigen 4; Fcy, Fc receptor γ; IL-6, interleukin 6; IL-10, interleukin 10; IL-17F, interleukin 17F; ICOSL, Inducible T-cell Costimulator Ligand; PI3K, phosphoinositide 3-kinase; PPE, porcine pancreatic elastase; and Tec, Tec protein tyrosine kinase.

factor-1α pathway in clinical AAA ($P < 0.052$) fail to reach the formal threshold for significance, yet this phenomenon may reflect a power problem because this pathway has previously been associated with AAA disease²⁸ as well as with AAA rupture.¹⁶

Metabolic Reprogramming and AAA Disease

The prominent metabolic signatures in clinical AAA disease and the AngII model (Figures 4 and 5) appear unique for AAA because they are not observed

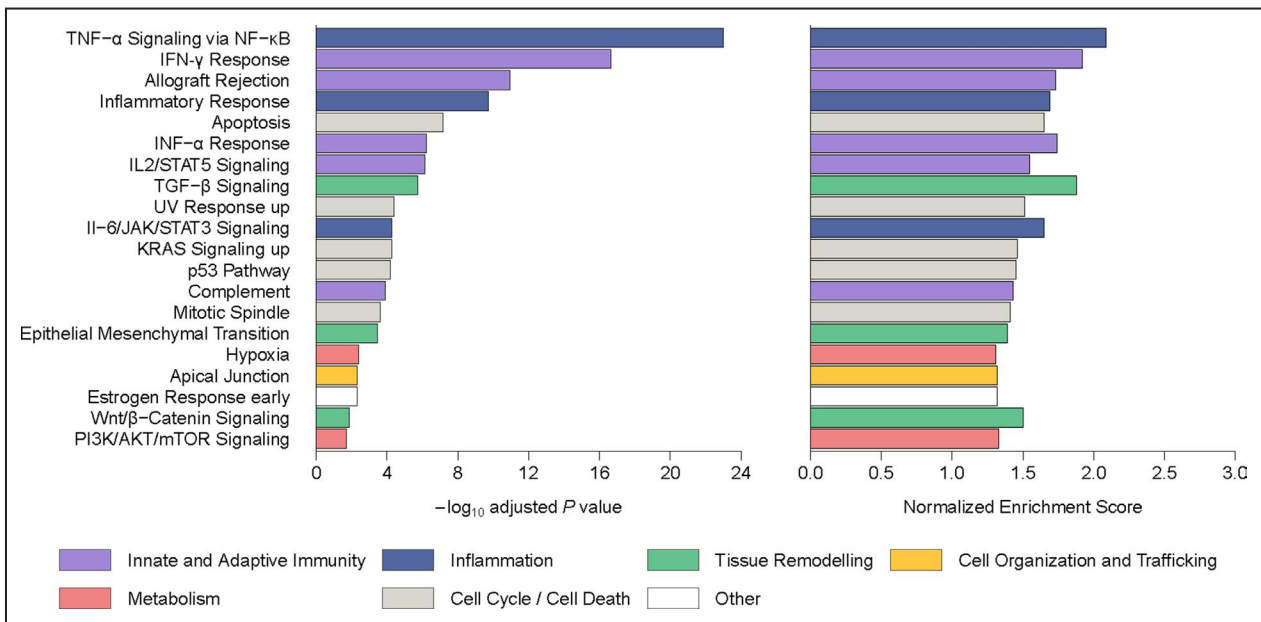


Figure 6. Gene set enrichment analysis of human AAA.

Gene classes overrepresented in the transcriptome of human AAA vs. control aorta. P values and normalized enrichment scores indicate probability and the relative degree of overrepresentation. AAA indicates abdominal aortic aneurysm; AKT, protein kinase B; IFN α , interferon α 1; IL-2, interleukin 2; IL-6, interleukin 6; JAK, Janus Kinase; KRAS, K-RAS; mTOR, mammalian target of rapamycin; PI3K, phosphoinositide 3-kinase; STAT5, Signal Transducer and Activator of Transcription-5; TGF- β , transforming growth factor β ; UV, Ultra Violet; and Wnt/ β -Catenin Signaling.

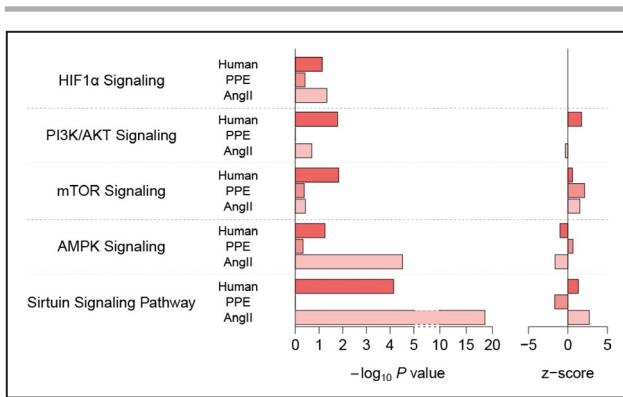


Figure 7. Activation status of the metabolic master switches in human AAA, and the PPE and AngII models. AAA indicates abdominal aortic aneurysm; AKT, protein kinase B; AMPK, AMP-activated protein kinase; AngII, angiotensin II; HIF1 α , hypoxia-induced factor-1 α ; mTOR, mammalian target of rapamycin; PI3K, phosphoinositide 3-kinase; and PPE, porcine pancreatic elastase.

in aneurysms of the ascending aorta.²⁹ A critical question is whether this metabolic signature with a predicted suppression (negative Z-scores) of oxidative phosphorylation (note that direction was not available for the glycolytic pathways) is part of the causative pathways driving disease progression. Alternative, and non-exclusive explanations are that the signature reflects a compensatory (regenerative) mechanism, or a neutral, bystander phenomenon. To address this aspect, we performed a rescue trial (ie, the intervention was initiated 1 week after start of the AngII infusion) with the potent glycolysis inhibitor PFK15. The metabolic impact of 6-phosphofructo-2-kinase/fructose-2,6-bisphosphatase 3 (PFKFB3) inhibition by PFK15 is clearly illustrated by the compensatory upregulation of aneurysm wall fructose-1,6-bisphosphatase 1 gene expression, and by reduced weight gain and reduced

blood glucose levels (Table 3). The rescue intervention reduced aortic dilatation ($P < 0.044$, Figure 8A) and aneurysm formation to 25% (PFK15 group) vs. 71% (vehicle group, Table 3). One mouse (in the AngII+PFK15 group) died of aortic rupture at day 27. PFK15 rescue treatment did not influence (day 28) expression of key inflammatory mediators, proteases, or fibrillar collagen (Figure 9), but prevented the AngII-induced drop in α -smooth muscle cell actin/vimentin ratio (Figure 8B).

DISCUSSION

The AAA is an enigmatic pathology.^{30,31} The disease generally remains clinically silent until manifested by an insidious and life-threatening rupture.³² As a consequence, most diagnosed intact AAA reflect longstanding disease, diagnosed as a coincidental finding during abdominal imaging, or a finding that results from active screening. By the same token, the actual mechanism(s) causing and driving the disease remain unclear, although epidemiological data, and the presence of clear (diffuse) genetic signals³³ and familial clustering,³⁴ imply that the disease results from complex gene–environment interactions with smoking and male sex as critical cofactors.³⁵

Remarkably little is known about the molecular basis of AAA disease. Available molecular insight largely relies on data derived from surgical specimens that were collected during open aneurysm repair (ie, larger aneurysms that represent late-stage disease). Assumptions on disease initiation and the earlier disease stages mainly rely on extrapolation of the pathological observations from late-stage disease, and on data derived from rodent models of AAA, in particular the PPE model and the AngII model. Although these 2 models are widely applied, contrasting outcomes for

Table 3. Effect of PFK15 (a PFKFB3 Glycolysis Inhibitor) Rescue Treatment on the Aortic Wall Characteristics and Gene Expression, and on Body Weight and Blood Glucose Levels (Day 28)

	Vehicle (Reference) n=6	AngII n=14	AngII + PFK15 n=12	P Value (AngII vs. AngII + PFK15)
Aneurysm formed (%)	0%	71%	25%	0.009
Elastin degradation score*	0	2	1	0.046
α -Smooth muscle cell actin expression†	1.00 [0.76–1.24]	0.31 [0.21–0.49]	0.73 [0.20–0.85]	ns
Fructose-1,6-bisphosphatase 1 expression†	0.76 [0.42–1.83]	0.20 [0.12–0.42]	0.78 [0.23–3.06]	0.016
Change in body weight vs. day 0 (g)	+1.0 [0.00–2.00]	+1.5 [1.00–2.00]	+0.1 [–0.50 to 1.00]	0.008
Blood glucose (mmol/L)	8.0 [6.40–9.10]	6.8 [5.65–7.90]	5.4 [4.80–5.90]	0.021

Data are presented as percent or median [interquartile range]. AngII indicates angiotensin II; ns, not significant; and PFK15, 1-(4-pyridinyl)-3-(2-quinolinyl)-2-propan-1-one.

*0: Intact elastic laminae, 1: Elastic laminae breaks and thinning, 2: Lost elastic laminae.

†Expression relative to Tata-box binding protein.

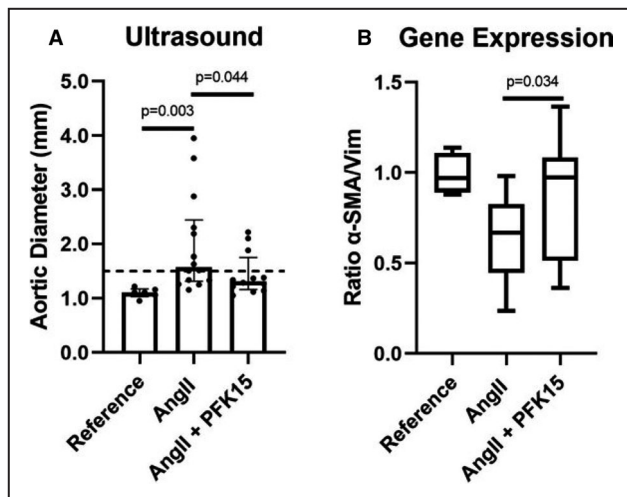


Figure 8. Impact of rescue treatment with the glycolysis inhibitor PFK15 in the AngII model.

Rescue treatment reduces aortic dilatation in the AngII model. **A**, Day- 28 maximal aorta diameters (median with interquartile range [mm]) measured by ultrasound. (bars: median, whiskers: interquartile ranges, dots: individual cases). **B**, PFK15 rescue-treatment preserves the vascular mesenchymal cell phenotype (boxplot horizontal line: median, box: lower and upper quartile, whiskers: range). AngII indicates angiotensin II; PFK15, 1-(4-pyridinyl)-3-(2-quinolinyl)-2-propen-1-one; α -SMA, α -smooth muscle cell actin; and Vim, vimentin.

pharmaceutical interventions performed in these models and the actual clinical context imply incomplete mimicry between the models and clinical disease.⁴ In light of this aspect, we considered an evaluation of parallel and incongruent genetic signals between clinical disease, and the 2 most commonly used models relevant.

Morphologic analogies and contrasts of clinical and experimental aneurysms were first inventoried through Movat pentachrome staining, a staining that provides optimal appreciation of the various structural aspects of the vascular wall.³⁶ Staining of human AAA illustrates the extreme extent of vascular remodeling in end-stage AAA disease. In fact, AAA tissue is characterized by disappearance of the characteristic 3-layered aortic wall structure, full loss of elastic laminae; deposition of a condensed, collagenous fibrous matrix, adventitial fatty degeneration, and appearance of follicle-like structures at the level of the former outer media. Histomorphologic analyses of the *experimental* AAA models were clearly distinct from *clinical* AAA disease. It was concluded that the actual aortic dilatation in the AngII model relates to the presence of a large intramural hematoma, an observation coinciding with previous conclusions that the model should actually be considered a dissection-induced model of aortic dilatation.¹⁰ Actual aortic aneurysm formation was observed in the PPE model. However, aneurysm formation was limited to the first 2 weeks following PPE exposure;

after which the aneurysm stabilizes as result of fibrotic changes in the wall. Histomorphologically, both models lacked the full characteristics of end-stage clinical disease (transmural fibrosis with extensive loss of smooth muscle cells and elastin, follicle formation, and fatty degeneration).

Despite the contrasting histological findings, there were clear overlaps for the genomic responses associated with clinical and experimental AAA disease, in particular the AngII model. The genomic signature of human AAA disease was dominated by a comprehensive activation of (pro)inflammatory pathways, and a particularly strong signal implying metabolic reprogramming (glycolytic shift). A similar overt metabolic and inflammatory response was observed for the AngII model.

In contrast to the AngII model, the PPE model associates with a transient genomic response with a clear (inflammatory) signature at day 7, but normalization of the genomic signal at day 14.

On the basis of this gross interpretation of the genomic responses, one could speculate that the AngII model is more representative for late-stage AAA disease with metabolic reprogramming and active ongoing fibrosis, and that the postinjury stages of the PPE model reflect quiescent fibrosis with minimal genetic signal. Consequently, the PPE model appears better positioned to study the earlier (initiating) stages of the disease.

The predicted strong genomic metabolic signature for clinical AAA disease and the AngII model is remarkable and novel, and appears AAA-specific since a similar signature is not observed for degenerative aneurysms of the ascending aorta.²⁹ A phenotypical glycolytic metabolic signature for AAA is confirmed by an enhanced AAA wall ¹⁸F-fluoro-deoxy-D-glucose uptake on positron emission tomography scans, an observation consistent with increased glycolytic activity in the AAA wall.³⁷ Following up on the enhanced ¹⁸F-fluoro-deoxy-D-glucose uptake in human AAA, Tsuruda et al.³⁸ hypothesized that enhanced glycolysis associates with AAA disease, and showed that the glycolysis inhibitor 2-deoxyglucose attenuates aortic dilatation after periaortic application of CaCl₂ and reduced the aneurysmal formation in the AngII model.

It could be speculated that the metabolic responses in clinical AAA disease and the AngII model are part of a fibrotic genomic signature as implied by the histological findings. Adaption of a glycolytic phenotype (including activated sirtuin signaling) in the mesenchymal cell population has now been recognized as a key driver and perpetuator of profibrotic responses.^{39,40} In fact, interference with glycolytic switching effectively prevents tissue fibrosis in experimental models.⁴¹ A further, and nonexclusive explanation for the dominant metabolic signature in clinical AAA disease and

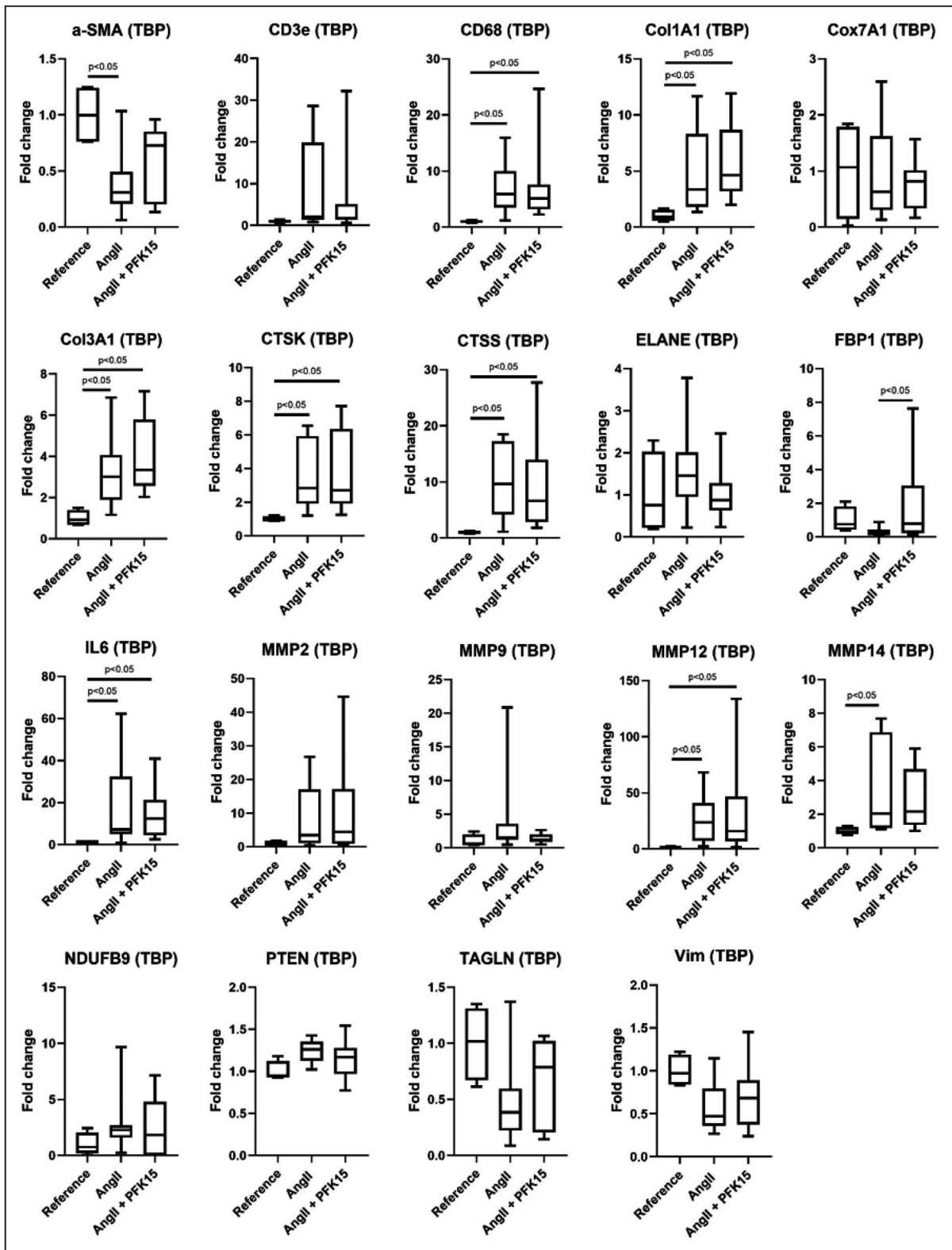


Figure 9. Boxplots indicating the relative (control median=1) gene expression (aortic tissue) in the reference aorta, the AngII control, and the intervention group.

Horizontal line: median, box: lower and upper quartile and whiskers: range. AngII indicates angiotensin II; CD68, cluster of differentiation 68; Col1A1, ColaA1; Col3A1, collagen 3A1; Cox7A1, cytochrome C oxidase subunit 7A1; CTSK, cathepsin K; CTSS, cathepsin S; ELANE, elastase, neutrophil expressed; FBP1, fructose-1,6-bisphosphatase 1; IL6, interleukin 6; MMP, matrix metalloproteinase; NDUFB9, NADH dehydrogenase 1 β subcomplex subunit 9; PFK15, 1-(4-pyridinyl)-3-(2-quinolinyl)-2-propen-1-one; PTEN, phosphatase and tensin homolog; α -SMA, smooth muscle cell actin; TAGLN, transgelin; TBP, TATA-box binding protein; and Vim, vimentin.

Downloaded from <http://ahajournals.org> by on March 22, 2022

the AngII model is that the signature mirrors leukocyte activation status/differentiation. In the context of inflammation, glycolytic switching plays crucial roles in processes associated with cell activation and phenotypical switching.⁴² In fact, metabolic switching is a critical aspect for processes such as T cell activation⁴³ and macrophage polarization (M1/M2).⁴⁴

In this light, the question arose whether the metabolic responses in clinical AAA disease are part of a beneficial compensatory regulatory mechanism delaying disease progression, or alternatively whether the responses drive disease progression.⁴⁵ To test the biological relevance of the metabolic reprogramming on disease progression, a proof-of-principle trial with the highly potent competitive PFKFB3 inhibitor PFK-15 was performed in the AngII model. The PFKFB family of enzymes drives the synthesis of fructose-2,6-biphosphate, the principal endogenous allosteric activator of 6-phosphofructo-1-kinase, 1 of the key rate-limiting enzymes of the glycolytic pathway. Among the 4 isoforms of PFKFBs, the PFKFB3 isoform has the highest kinase-to-phosphatase ratio, and is the dominant form in the vasculature, leukocytes, as well as many transformed cells (PMID: 15170386).⁴⁶ PFKFB3 is considered a metabolic master-switch that controls the balance between oxidative phosphorylation and aerobic glycolysis.²⁵

The PFK-15 treatment was set up as a rescue trial with treatment initiated on day 7 after the start of the AngII infusion to better mimic the actual clinical context. This intervention study showed that interference with glycolytic switching quenches disease progression, through a mechanism that appears independent from an effect on key inflammatory or proteolytic pathways and may involve interference with mesenchymal cell-phenotype switching. Conclusions of the metabolic intervention align with the observations for metformin treatment, both metabolically (lowering of blood glucose levels, weight loss)⁴⁷ as well as with respect to its reported effects on the aneurysm wall.^{48,49}

In the context of prominent metabolic signatures of clinical AAA disease and the AngII model, and its apparent role in disease progression, we performed a focused evaluation of known key-metabolic regulators (Figure 6). Again, clear contrasts were observed for the elastase model; however, Ingenuity Pathway Analysis also predicted contrasting directionality for phosphoinositide 3-kinase/protein kinase B signaling and an absent signal for AMP-activated protein kinase signaling in clinical AAA. In the light of the confirmed and validated activation of the hypoxia-induced factor-1 α pathway in growing AAA²⁸ and a further activation in end-stage AAA,¹⁶ it is likely that the failure for the hypoxia-induced factor-1 α signal to reach formal significance reflects a power problem.

The prominent inflammatory aspects of AAA disease are reflected in a second cluster of genomic responses, which converges at aspects of inflammation. The inflammatory signature of clinical AAA disease best aligns with that of a general pro-inflammatory response, involving aspects of both the innate and adaptive immune response. This observation is consistent with earlier conclusions that the inflammatory phenotype of AAA disease should be considered general pro-inflammatory, rather than specifically Th1 or Th2 polarized.⁵⁰ Compared with the human signature, murine signatures were more skewed to an adaptive immune response. Contrasting directionality was predicted for some of the genomic responses in the murine models (in particular the PPE model) versus clinical AAA disease. Although the contrasts between clinical and AAA disease may reflect aspects such as nuances in the inflammatory landscapes between clinical and experimental AAA disease, species-related differences in inflammatory responses⁵¹ and/or disease stage,⁵² as well as the apparent self-limiting nature of the PPE model, it cannot be excluded that (part of) the contrast between the actual pathology and the experimental models is an artifact caused by the critical requirement for Th1-skewed genetic-backgrounds⁵³ in order for experimental aneurysms to develop in the murine models.⁸

LIMITATIONS

The focus of the study is on a comparison of clinical disease and the 2 most commonly used murine AAA models. This study did not include an evaluation of the calcium-salt-induced AAA murine model, nor the more recently published topical application of elastase rather than of intraluminal elastase perfusion⁵⁴ or models reported in rat, rabbit, and larger animals.

The aim of this study was the identification of generic processes present in clinical disease and its most commonly used models by means of pathway analysis. As such, it relies on integration of whole tissue (bulk) RNA expression data, and conclusions from this evaluation are based on a high level of data aggregation. Accordingly, the study lacks information on individual genes, cells, and molecules, and is prone to interference related to differences in cellular composition. The focus on RNA expression further ignores aspects of pretranslational (miRNA, long non-coding RNAs)^{55,56} and posttranslational regulation and possible roles for cells without active protein synthesis (such as neutrophils).

Moreover, a focus on RNA expression in non-steady-state conditions skews the data to the early aspects of the response at different time points. This latter aspect may explain the apparent incongruence

of normalization of the genomic profile and the histological aspects.

A particular challenge for the clinical AAA data is the definition of the appropriate controls. Controls used in the clinical data set were elderly organ donors with an age range matching that of the patients with AAA. As such, most control samples will present with aspects of the atherosclerotic process. Although the potential interference of this aspect is partially eliminated by the comparison with the animal model, this remains a potential source of confounding. A further limitation is the very limited number of female patients (3%) in the AAA cohort (33% in the controls). As such, no conclusion can be drawn with regard to a potential impact of sex on the genetic signatures. Finally, information on the earlier stages of clinical AAA disease is missing. As such, any conclusions with regard to the extrapolation of the data from the PPE model to the early disease stages of human AAA are fully speculative.

In conclusion, this evaluation shows parallel inflammatory responses in clinical AAA disease and the 2 models. Despite the clear morphologic differences, the RNA expression data showed remarkable parallels between clinical AAA disease and the AngII model, with a notable strong signal for metabolic switching. Results from the PFKFB3 intervention trial suggest that a glycolytic switch drives AAA progression. This conclusion provides a rationale for the putative beneficial effects of metformin therapy as well as for the so-far unexplained negative association between diabetic disease and AAA progression.

The transient transcriptional responses and spontaneous recovery classify the PPE model as a model of disease initiation that could be of benefit for identifying aspects involved in disease perpetuation. Given the contrasts between clinical established disease and the inherent differences between the models, the data do not support the concept of combining different models to improve the translatability of study findings; however, they do provide a rationale for a better positioning of the 2 models.

ARTICLE INFORMATION

Received January 26, 2021; accepted May 19, 2021.

Affiliations

Department of Vascular Surgery, HELIOS Klinikum Krefeld, Krefeld, Germany (G.G.); Institute of Laboratory Medicine, Ludwig-Maximilians-University Munich, Munich, Germany (B.H.N., D.T., L.M.H.); Department of Medical Cell Biology, Uppsala University, Uppsala, Sweden (A.B., M.B.A., M.P., D.W.); Department of Vascular and Endovascular Surgery, Technical University Munich, Munich, Germany (A.B., L.M.); University Centre for Vascular Medicine, University Hospital Carl Gustav Carus, Technical University Dresden, Dresden, Germany (A.M., S.L.); Department Medical Biochemistry, Amsterdam University Medical Centers, Amsterdam Cardiovascular Sciences, University of Amsterdam, Amsterdam, The Netherlands (V.d.W.); Queensland Research Centre for Peripheral Vascular Disease, College of

Medicine and Dentistry, James Cook University, Townsville, Qld., Australia (J.G.); Department of Surgical Sciences, Section of Vascular Surgery, Uppsala University, Uppsala, Sweden (A.W.); and Department of Vascular Surgery, Leiden University Medical Center (LUMC), Leiden, The Netherlands (J.H.L.).

Sources of Funding

Dr Gäbel received funding from the German Society for Vascular Surgery ("Aortenstipendium"). Dr Wågsäter received grants from the Swedish Research Council (grant no. 2019-01673) and Swedish Heart and Lung Foundation (grant no. 20190556). Dr Golledge received funding from the Queensland Government, National Health and Medical Research Council (IDs 1020955, 1021416, 1063476 and 1000967) and Townsville Hospital Private Practice Trust for this work. Dr Teupser and Dr Holdt received funding from the Deutsche Forschungsgemeinschaft as part of the CRC 1123 (B1, B5) and the CRC 267 (A07, B04).

Disclosures

None.

Supplementary Material

Supplementary material

REFERENCES

1. Wanhaien A, Verzini F, Van Herzelee I, Allaire E, Bown M, Cohnert T, Dick F, van Herwaarden J, Karkos C, Koelemay M, et al. Editor's choice - european society for vascular surgery (ESVS) 2019 clinical practice guidelines on the management of abdominal aorto-iliac artery aneurysms. *Eur J Vasc Endovasc Surg*. 2019;57:8–93. DOI: 10.1016/j.ejvs.2018.09.020.
2. Baxter BT, Terrin MC, Dalman RL. Medical management of small abdominal aortic aneurysms. *Circulation*. 2008;117:1883–1889. DOI: 10.1161/CIRCULATIONAHA.107.735274.
3. Lederle FA. Abdominal aortic aneurysm: still no pill. *Ann Intern Med*. 2013;159:852–853. DOI: 10.7326/0003-4819-159-12-201312170-00012.
4. Lindeman JH, Matsumura JS. Pharmacologic management of aneurysms. *Circ Res*. 2019;124:631–646. DOI: 10.1161/CIRCRESAHA.118.312439.
5. Azuma J, Asagami T, Dalman R, Tsao PS. Creation of murine experimental abdominal aortic aneurysms with elastase. *J Vis Exp*. 2009;29:1280. DOI: 10.3791/1280.
6. Busch A, Holm A, Wagner N, Ergün S, Rosenfeld M, Otto C, Baur J, Kellersmann R, Lorenz U. Extra- and intraluminal elastase induce morphologically distinct abdominal aortic aneurysms in mice and thus represent specific subtypes of human disease. *J Vasc Res*. 2016;53:49–57. DOI: 10.1159/000447263.
7. Thompson RW, Curci JA, Ennis TL, Mao D, Pagano MB, Pham CT. Pathophysiology of abdominal aortic aneurysms: insights from the elastase-induced model in mice with different genetic backgrounds. *Ann N Y Acad Sci*. 2006;1085:59–73. DOI: 10.1196/annals.1383.029.
8. Sénémaud J, Caligiuri G, Etienne H, Delbosc S, Michel JB, Coscas R. Translational relevance and recent advances of animal models of abdominal aortic aneurysm. *Arterioscler Thromb Vasc Biol*. 2017;37:401–410. DOI: 10.1161/ATVBAHA.116.308534.
9. Saraff K, Babamusta F, Cassis LA, Daugherty A. Aortic dissection precedes formation of aneurysms and atherosclerosis in angiotensin II-infused, apolipoprotein E-deficient mice. *Arterioscler Thromb Vasc Biol*. 2003;23:1621–1626. DOI: 10.1161/01.ATV.0000085631.76095.64.
10. Trachet B, Aslanidou L, Piersigilli A, Fraga-Silva RA, Sordet-Dessimoz J, Villanueva-Perez P, Stamparoni MFM, Stergiopoulos N, Segers P. Angiotensin II infusion into ApoE^{-/-} mice: a model for aortic dissection rather than abdominal aortic aneurysm? *Cardiovasc Res*. 2017;113:1230–1242. DOI: 10.1093/cvr/cvx128.
11. Marinković G, Hibender S, Hoogenboezem M, van Broekhoven A, Girgorie AF, Bleeker N, Hamers AAJ, Stap J, van Buul JD, de Vries CJM, et al. Immunosuppressive drug azathioprine reduces aneurysm progression through inhibition of Rac1 and c-Jun-terminal-N-kinase in endothelial cells. *Arterioscler Thromb Vasc Biol*. 2013;33:2380–2388. DOI: 10.1161/ATVBAHA.113.301394.

12. Rush C, Nyara M, Moxon JV, Trollope A, Cullen B, Golledge J. Whole genome expression analysis within the angiotensin II-apolipoprotein E deficient mouse model of abdominal aortic aneurysm. *BMC Genom.* 2009;10:298. DOI: 10.1186/1471-2164-10-298.
13. Li DY, Busch A, Jin H, Chernogubova E, Pelisek J, Karlsson J, Sennblad B, Liu S, Lao S, Hofmann P, et al. H19 induces abdominal aortic aneurysm development and progression. *Circulation.* 2018;138:1551–1568. DOI: 10.1161/CIRCULATIONAHA.117.032184.
14. Maegdefessel L, Spin JM, Raaz U, Eken SM, Toh R, Azuma J, Adam M, Nagakami F, Heymann HM, Chernogubova E, et al. miR-24 limits aortic vascular inflammation and murine abdominal aneurysm development. *Nat Commun.* 2014;5:5214. DOI: 10.1038/ncomms6214.
15. Biros E, Gäbel G, Moran CS, Schreurs C, Lindeman JHN, Walker PJ, Nataatmadja M, West M, Holdt LM, Hinterseher I, et al. Differential gene expression in human abdominal aortic aneurysm and aortic occlusive disease. *Oncotarget.* 2015;6:12984–12996. DOI: 10.18632/oncotarget.3848.
16. Gäbel G, Northoff BH, Weinzierl I, Ludwig S, Hinterseher I, Wilfert W, Teupser D, Doderer SA, Bergert H, Schönleben F, et al. Molecular fingerprint for terminal abdominal aortic aneurysm disease. *J Am Heart Assoc.* 2017;6:e006798. DOI: 10.1161/JAHA.117.006798.
17. Ritchie ME, Phipson B, Wu D, Hu Y, Law CW, Shi W, Smyth GK. limma powers differential expression analyses for RNA-seq and microarray studies. *Nucleic Acids Res.* 2015;43:e47. DOI: 10.1093/nar/gkv007.
18. Hoffmann S, Otto C, Kurtz S, Sharma CM, Khaitovich P, Vogel J, Stadler PF, Hackermüller J. Fast mapping of short sequences with mismatches, insertions and deletions using index structures. *PLoS Comput Biol.* 2009;5:e1000502. DOI: 10.1371/journal.pcbi.1000502.
19. Liao Y, Smyth GK, Shi W. featureCounts: an efficient general purpose program for assigning sequence reads to genomic features. *Bioinformatics.* 2014;30:923–930. DOI: 10.1093/bioinformatics/btt656.
20. Love MI, Huber W, Anders S. Moderated estimation of fold change and dispersion for RNA-seq data with DESeq2. *Genome Biol.* 2014;15:550. DOI: 10.1186/s13059-014-0550-8.
21. Krämer A, Green J, Pollard J Jr, Tugendreich S. Causal analysis approaches in ingenuity pathway analysis. *Bioinformatics.* 2014;30:523–530. DOI: 10.1093/bioinformatics/btt703.
22. Sergushichev A. An algorithm for fast preranked gene set enrichment analysis using cumulative statistic calculation. *bioRxiv.* Preprint posted June 20, 2016. DOI: 10.1101/060012.
23. Subramanian A, Tamayo P, Mootha VK, Mukherjee S, Ebert BL, Gillette MA, Paulovich A, Pomeroy SL, Golub TR, Lander ES, et al. Gene set enrichment analysis: a knowledge-based approach for interpreting genome-wide expression profiles. *Proc Natl Acad Sci USA.* 2005;102:15545–15550. DOI: 10.1073/pnas.0506580102.
24. Liberzon A, Birger C, Thorvaldsdóttir H, Ghandi M, Mesirov JP, Tamayo P. The molecular signatures database (MSigDB) hallmark gene set collection. *Cell Syst.* 2015;1:417–425.
25. Clem BF, O'Neal J, Tapolsky G, Clem AL, Imbert-Fernandez Y, Kerr DA, Klarer AC, Redman R, Miller DM, Trent JO, et al. Targeting 6-phosphofructo-2-kinase (PFKFB3) as a therapeutic strategy against cancer. *Mol Cancer Ther.* 2013;12:1461–1470. DOI: 10.1158/1535-7163.MCT-13-0097.
26. Pfaffl MW. Relative quantification. In: Dorak MT, ed. *Real-Time PCR.* La Jolla, CA: International University Line; 2006:63–82.
27. Glazko AJ. Effect of blood protease and trypsin inhibitor on the clotting mechanism. *J Clin Invest.* 1947;26:364–369.
28. Wang W, Xu B, Xuan H, Ge Y, Wang Y, Wang L, Huang J, Fu W, Michie SA, Dalman RL. Hypoxia-inducible factor 1 in clinical and experimental aortic aneurysm disease. *J Vasc Surg.* 2018;68:1538–1550. DOI: 10.1016/j.jvs.2017.09.030.
29. Sulkava M, Raitoharju E, Mennander A, Levula M, Seppälä I, Lyytikäinen L-P, Järvinen O, Illig T, Klopp N, Mononen N, et al. Differentially expressed genes and canonical pathways in the ascending thoracic aortic aneurysm - The Tampere Vascular Study. *Sci Rep.* 2017;7:12127. DOI: 10.1038/s41598-017-12421-4.
30. Dalman RL, Wanhainen A, Mani K, Modarai B. Top 10 candidate aortic disease trials. *J Intern Med.* 2020;288:23–37. DOI: 10.1111/joim.13042.
31. Lindeman JH. The pathophysiologic basis of abdominal aortic aneurysm progression: a critical appraisal. *Expert Rev Cardiovasc Ther.* 2015;13:839–851. DOI: 10.1586/14779072.2015.1052408.
32. Sakalilhan N, Michel JB, Katsargyris A, Kuivaniemi H, Defraigne JO, Nchimi A, Powell JT, Yoshimura K, Hultgren R. Abdominal aortic aneurysms. *Nat Rev Dis Primers.* 2018;4:34. DOI: 10.1038/s41572-018-0030-7.
33. Pinard A, Jones GT, Milewicz DM. Genetics of thoracic and abdominal aortic diseases. *Circ Res.* 2019;124:588–606. DOI: 10.1161/CIRCRESAHA.118.312436.
34. van de Luijngaarden KM, Rouwet EV, Hoeks SE, Stolker RJ, Verhagen HJ, Majoor-Krakauer D. Risk of abdominal aortic aneurysm (AAA) among male and female relatives of AAA patients. *Vasc Med.* 2017;22:112–118. DOI: 10.1177/1358863X16686409.
35. Cornuz J, Sidoti Pinto C, Tevearai H, Egger M. Risk factors for asymptomatic abdominal aortic aneurysm: systematic review and meta-analysis of population-based screening studies. *Eur J Public Health.* 2004;14:343–349. DOI: 10.1093/eurpub/14.4.343.
36. Otsuka F, Joner M, Prati F, Virmani R, Narula J. Clinical classification of plaque morphology in coronary disease. *Nat Rev Cardiol.* 2014;11:379–389. DOI: 10.1038/nrcardio.2014.62.
37. Timur UT, van Herwaarden JA, Mihajlovic D, De Jong P, Mali W, Moll FL. (18)F-FDG PET scanning of abdominal aortic aneurysms and correlation with molecular characteristics: a systematic review. *EJNMMI Res.* 2015;5:76. DOI: 10.1186/s13550-015-0153-8.
38. Tsuruda T, Hatakeyama K, Nagamachi S, Sekita Y, Sakamoto S, Endo GJ, Nishimura M, Matsuyama M, Yoshimura K, Sato Y, et al. Inhibition of development of abdominal aortic aneurysm by glycolysis restriction. *Arterioscler Thromb Vasc Biol.* 2012;32:1410–1417. DOI: 10.1161/ATVBAHA.111.237065.
39. Zhao X, Kwan JYY, Yip K, Liu PP, Liu FF. Targeting metabolic dysregulation for fibrosis therapy. *Nat Rev Drug Discov.* 2020;19:57–75. DOI: 10.1038/s41573-019-0040-5.
40. Morigi M, Perico L, Benigni A. Sirtuins in renal health and disease. *J Am Soc Nephrol.* 2018;29:1799–1809. DOI: 10.1681/ASN.2017111218.
41. Xie N, Tan Z, Banerjee S, Cui H, Ge J, Liu RM, Bernard K, Thannickal VJ, Liu G. Glycolytic reprogramming in myofibroblast differentiation and lung fibrosis. *Am J Respir Crit Care Med.* 2015;192:1462–1474. DOI: 10.1164/rccm.201504-0780OC.
42. Arts RJ, Gresnigt MS, Joosten LA, Netea MG. Cellular metabolism of myeloid cells in sepsis. *J Leukoc Biol.* 2017;101:151–164. DOI: 10.1189/jlb.4MR0216-066R.
43. Pearce EL, Poffenberger MC, Chang CH, Jones RG. Fueling immunity: insights into metabolism and lymphocyte function. *Science.* 2013;342:1242454. DOI: 10.1126/science.1242454.
44. Rodríguez-Prados JC, Través PG, Cuenca J, Rico D, Aragónés J, Martín-Sanz P, Cascante M, Boscá L. Substrate fate in activated macrophages: a comparison between innate, classic, and alternative activation. *J Immunol.* 2010;185:605–614. DOI: 10.4049/jimmunol.0901698.
45. Lindeman JH, Ashcroft BA, Beenakker JW, van Es M, Koekkoek NB, Prins FA, Tielemans JF, Abdul-Hussien H, Bank RA, Oosterkamp TH. Distinct defects in collagen microarchitecture underlie vessel-wall failure in advanced abdominal aneurysms and aneurysms in Marfan syndrome. *Proc Natl Acad Sci USA.* 2010;107:862–865. DOI: 10.1073/pnas.0910312107.
46. Rider MH, Bertrand L, Vertommen D, Michels PA, Rousseau GG, Hue L. 6-phosphofructo-2-kinase/fructose-2,6-bisphosphatase: head-to-head with a bifunctional enzyme that controls glycolysis. *Biochem J.* 2004;381:561–579. DOI: 10.1042/BJ20040752.
47. Seifarth C, Schehler B, Schneider HJ. Effectiveness of metformin on weight loss in non-diabetic individuals with obesity. *Exp Clin Endocrinol Diabetes.* 2013;121:27–31. DOI: 10.1055/s-0032-1327734.
48. Rangarajan S, Bone NB, Zmijewska AA, Jiang S, Park DW, Bernard K, Locy ML, Ravi S, Deshane J, Mannon RB, et al. Metformin reverses established lung fibrosis in a bleomycin model. *Nat Med.* 2018;24:1121–1127. DOI: 10.1038/s41591-018-0087-6.
49. Yu X, Jiang D, Wang J, Wang R, Chen T, Wang K, Durgahee MSA, Wei X, Cao S. Metformin prescription and aortic aneurysm: systematic review and meta-analysis. *Heart.* 2019;105:1351–1357. DOI: 10.1136/heartjnl-2018-314639.
50. Lindeman JH, Abdul-Hussien H, Schaapherder AF, Van Bockel JH, Von der Thüsen JH, Roelen DL, Kleemann R. Enhanced expression and activation of pro-inflammatory transcription factors distinguish aneurysmal from atherosclerotic aorta: IL-6 and IL-8-dominated inflammatory responses prevail in the human aneurysm. *Clin Sci (Lond).* 2008;114:687–697. DOI: 10.1042/CS20070352.
51. Mestas J, Hughes CC. Of mice and not men: differences between mouse and human immunology. *J Immunol.* 2004;172:2731–2738. DOI: 10.4049/jimmunol.172.5.2731.

-
52. Seok J, Warren HS, Cuenca AG, Mindrinos MN, Baker HV, Xu W, Richards DR, McDonald-Smith GP, Gao H, Hennessy L, et al. Inflammation and host response to injury, large scale collaborative research program. genomic responses in mouse models poorly mimic human inflammatory diseases. *Proc Natl Acad Sci USA*. 2013;110:3507–3512. DOI: 10.1073/pnas.1222878110.
 53. Watanabe H, Numata K, Ito T, Takagi K, Matsukawa A. Innate immune response in Th1- and Th2-dominant mouse strains. *Shock*. 2004;22:460–466. DOI: 10.1097/01.shk.0000142249.08135.e9.
 54. Bhamidipati CM, Mehta GS, Lu G, Moehle CW, Barbery C, DiMusto PD, Laser A, Kron IL, Upchurch GR Jr, Ailawadi G. Development of a novel murine model of aortic aneurysms using peri-adventitial elastase. *Surgery*. 2012;152:238–246. DOI: 10.1016/j.surg.2012.02.010.
 55. Iyer V, Rowbotham S, Biros E, Bingley J, Golledge J. A systematic review investigating the association of microRNAs with human abdominal aortic aneurysms. *Atherosclerosis*. 2017;261:78–89. DOI: 10.1016/j.atherosclerosis.2017.03.010.
 56. Wu ZY, Trenner M, Boon RA, Spin JM, Maegdefessel L. Long non-coding RNAs in key cellular processes involved in aortic aneurysms. *Atherosclerosis*. 2020;292:112–118. DOI: 10.1016/j.atherosclerosis.2019.11.013.

Supplement 1. Protocol Movat Pentachrome Staining:

Vascular Surgery Lab, Leiden University Medical Center.

Working solutions:

(A) 1% Alcian Blue Solution: 1 g Alcian Blue 8 GX (Merck, Burlington, US), 100 ml distilled water, 1 ml Glacial Acetic Acid (Sigma Aldrich, Saint Louis, US)

(B) Alkaline Alcohol solution: 10 ml Ammonium Hydroxide (Merck, Burlington, US), 90 ml Ethanol 100%.

(C) Elastic Hematoxylin Solution: 25 ml 10% Alcoholic Hematoxylin (J), 25 ml Ethanol 100%, 25 ml 10% Ferric Chloride (D), 25 ml Verhoeff's Iodine Solution (K).

(D) 10% Ferric Chloride Solution: 10 g Ferric Chloride (Sigma Aldrich, Saint Louis, US), 100 ml distilled water

(E) 5% Sodium Thiosulfate Solution: 5g Sodium Thiosulfate (Sigma Aldrich, Saint Louis, US), 100 ml distilled water

(F) Biebrich Scarlet/Acid Fuchsin solution: pre-made from ScyTek Laboratories (Logan, United States).

(G) 1% Acetic Acid Solution: 1 ml Glacial Acetic Acid, 99 ml distilled water

(H) 5% Aqueous Phosphotungstic Acid solution: 5 g Phosphotungstic Acid (Sigma Aldrich, Saint Louis, US), 100 ml distilled water

(I) 4% Alcoholic Saffron Solution: 4 g Saffron (Safranor Safran du Gâtinais, Échilleuses, France), 100 ml Ethanol 100%.

(J) 10% Alcoholic Hematoxylin Solution: 10 g Hematoxylin (Merck, Burlington, US), 100 ml Ethanol 100%

(K) Verhoeff's Iodine Solution: 2 g Iodine Crystals (Sigma Aldrich, Saint Louis, US), 4 g Potassium Iodide (Sigma Aldrich, Saint Louis, US), 100 ml distilled water

Protocol:

1. Deparaffinization and rehydration of slides.
2. Rinse slides in distilled water.
3. Stain in 2 changes with (A) , both times for 15-25 minutes.
4. Rinse slides in running warm to hot water until clear.
5. Place slides in (B) for 30 minutes, then rinse in running tap water.
6. Stain in (C) for 20 minutes.
7. Rinse in running warm tap water.
8. Differentiate in 2% aqueous (D) for 5 seconds-2 minutes.
9. Place slides in (E) for about 1 minute.
10. Wash in running tap water and rinse in distilled water.
11. Stain in (F) for 1-1.5 minutes.
12. Rinse in distilled water.
13. Rinse in (G) for 7-12 seconds.
14. Place slides in (H) for 7-12 minutes.
15. Rinse in distilled water.
16. Rinse in (G) for 8-10 seconds.
17. Place in 2 changes of Ethanol

100%. 18. Stain in (I) for 1.5 minute and quickly rinse in Ethanol 100%. 19. Dehydration of slides. Mount with Pertex.